Handling mode and polarization in fiber by fs-laser inscribed (de)multiplexer and silicon switch array

Kang Li[1,2†] , Min Yang[1,2†], Chengkun Cai[1,2†], Xiaoping Cao[1,2], Guofeng Yan[1,2], Guangze Wu[1,2], Yuanjian Wan[1,2] and Jian Wang[1,2*]

†Kang Li, Min Yang and Chengkun Cai contributed equally to this work.

*Correspondence:
jwang@hust.edu.cn

[1] Wuhan National Laboratory for Optoelectronics and School of Optical and Electronic Information, Huazhong University of Science and Technology, Wuhan, Hubei 430074, China
[2] Optics Valley Laboratory, Wuhan, Hubei 430074, China

Abstract

The emergence of dynamic optical switching has opened up new perspectives for lightening the ever growing load on the electrical switches and routers, to meet the increasing demand on high-speed and flexible data processing and management in fiber-optic communications. Despite diversity schemes of optical switching in the single-mode regime, multi-mode switching of the hybrid fiber and chip system enabled by photonic integrated circuits, especially for the fiber-chip-fiber system, is still an outstanding challenge. Here, we propose and demonstrate the mode and polarization transmission and switching fiber-chip-fiber system with few-mode fibers (FMFs), including the FMF links for mode- and polarization-division multiplexing data transmission, the femtosecond (fs)-laser inscribed 3-dimensional (3D) photonic lantern silica chip for (de)multiplexing and coupling between FMFs and chip, and the topology-optimized N × N non-blocking 2-dimensional (2D) silicon switch array chip for switching and routing. Using 30-Gbaud quadrature phase-shift keying signals on wavelength-division multiplexing (WDM) channels, the WDM-compatible hybrid mode/polarization transmission, switching and routing system with FMFs, fs-laser inscribed silica (de)multiplexing chip and silicon switch array chip are demonstrated in the experiment with favorable operation performance. The demonstration may open the door for developing robust multi-dimensional optical data processing in fiber-optic communication systems with versatile fibers and chips.

Keywords: Fiber-optic communications, Optical switching, Few-mode fiber, Femtosecond (fs) laser direct writing, Silicon photonics, Photonic integrated circuits

Introduction

Dynamic optical switching is of great significance to reduce the power consumption in high-capacity fiber-optic communication and data center networks [1, 2]. As the pivotal device, multi-port optical switch with low cost has attracted extensive attention, which has been applied in long-distance fiber-optic communications and photonic integrated on-chip networks [3, 4]. It is worth mentioning that the N × N non-blocking optical switch consisting of a certain number of 2 × 2 element switches and crossings has emerged as a powerful technique for a flexible and energy-saving

switching network [5–9]. Besides, a lot of integrated on-chip switching structures based on silicon-on-insulator (SOI) [10–12], InP [13, 14], and waveguide-based microelectromechanical system platforms [15] have been demonstrated, showing that high-density photonic integration is a promising approach. Among these, benefiting from the free carrier plasma dispersion, silicon electro-optical switches with complementary metal-oxide semiconductor (CMOS) compatibility have shown distinct advantages of compactness and fast switching time, becoming a promising technology for prospective high-speed optical switching networks [16, 17].

Meanwhile, in order to meet the demand for ever-increasing data traffic [18], numerous technique breakthroughs, such as wavelength-division multiplexing (WDM), polarization-division multiplexing (PDM), erbium-doped fiber amplifier (EDFA), high-order modulation formats, and coherent detection, have been applied in optical communications for gaining higher capacity. However, the data transmission capability of single-mode fiber (SMF) is rapidly approaching its nonlinear Shannon limit [18–21]. Since the spatial degree of freedom of lightwaves can be also considered as an independent physical dimension to enable efficient capacity scaling for fiber-optic communications [22–26]. Space-division multiplexing (SDM) in optical fibers, including SDM in multi-core fiber (MCF) and mode-division multiplexing (MDM) in few-mode fiber (FMF) has been proposed to address the coming "capacity crunch". In addition, the concept of SDM and MDM can also be extended to multi-mode waveguides for high-capacity on-chip optical interconnects [27–34]. Remarkably, modern optical communication technologies generally use fibers for optical data transmission, and photonic integrated chips for optical data processing. Hence, the hybrid applications of transmission and processing systems incorporating fibers and chips are inevitable trends of prospective optical communications. Traditionally, free-space discrete optical elements are employed for mode (de)multiplexing, which are complicated, cumbersome and unstable. Very recently, all-fiber mode-selective couplers, vertical grating couplers and photonic lanterns have been proposed for mode (de)multiplexing with impressive performance [35–38]. However, few research efforts have been paid to combine these FMFs, compact mode (de)multiplexers and silicon chips together to build an entire fiber-chip-fiber communication system with both optical data transmission and processing in the multi-mode regime. In this scenario, a laudable goal would be to develop an FMF-chip-FMF system.

In this paper, we propose and demonstrate an FMF-chip-FMF optical transmission and switching system with fs-laser inscribed (de)multiplexer and silicon switch array, enabling various functions of transmission, (de)multiplexing, switching and routing for hybrid mode/polarization multiplexing signals. Here, the hybrid mode/polarization switching from FMF to chip is achieved with the assist of fs-laser inscribed 3D silica chip acting as the mode/polarization (de)multiplexer. The 2D silicon chip makes use of the $N \times N$ non-blocking switch to perform the switching and routing functions. The topology-optimized $N \times N$ non-blocking switch with fewer 2×2 element switches and crossings, unlike the case in conventional non-blocking switch, facilitates dynamic switching of optical signals with low loss and low crosstalk. Furthermore, using 30-Gbaud quadrature phase-shift keying (QPSK) signals on multiple WDM channels, the demonstrated WDM-compatible hybrid mode/polarization FMF-chip-FMF transmission and

switching system shows favorable performance. The observed optical signal-to-noise ratio (OSNR) penalties are less than 4.5 dB at a bit-error rate (BER) of 3.8×10^{-3}.

Concept and devices

Concept

The concept and principle of the FMF-chip-FMF mode/polarization switching system are illustrated in Fig. 1, which contains three basic functions, i.e. mode/polarization demultiplexing, multi-port switching/routing, and mode/polarization multiplexing. The FMF transmission link is compatible with MDM and PDM, supporting N linear polarization (LP) modes and two polarizations. Firstly, the $2 \times N$ mode/polarizations are converted into two orthogonal LP_{01} modes at N output ports by the mode demultiplexer. After that, the polarization demultiplexer separates two orthogonal LP_{01} modes to two channels. Then, the polarization controller (PC) converts different polarizations of two channels to the same polarization. The $2 \times N$ mode/polarization channels can carry multiple data signals. The mode/polarization multiplexing and demultiplexing are reversible. In addition, the silicon integrated multi-port non-blocking switch array chip with topology optimization is composed of fewer switch units and crossings. The pivotal switch unit is a 2×2 thermo-optic Mach-Zehnder interferometer (MZI), enabling a flexible switch between two output ports and two input ports by thermal tuning.

Devices

Following the concept and principle, we construct the FMF-chip-FMF mode/polarization switching system. In the switch system, fs-laser inscribed (de)multiplexer on 3D silica chip and switch array on 2D silicon chip are key devices.
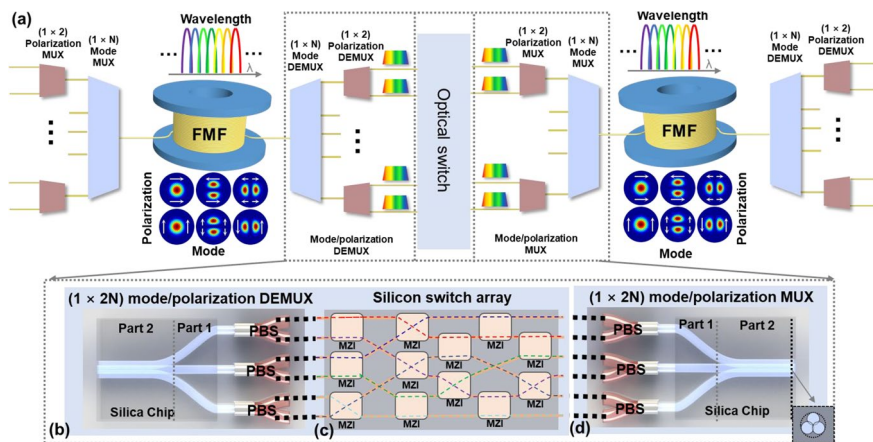

Fig. 1 Concept and principle of the FMF-chip-FMF mode/polarization switching system with fs-laser inscribed (de)multiplexer and silicon switch array. **a** The FMF-chip-FMF mode/polarization switching system with three basic functions, i.e. mode/polarization demultiplexing, multi-port switching/routing, and mode/polarization multiplexing. **b, d** The 1 × 2N mode/polarization (de)multiplexer consisting of a mode (de)multiplexer on the 3D silica chip and N PBSs. The inset in (**d**) shows the cross section of multimode port in the (de)multiplexer. **c** The topology-optimized 2N × 2N non-blocking switch on 2D silicon chip consisting of fewer 2 × 2 element switches and crossings. MUX: multiplexer; DEMUX: demultiplexer; MZI: Mach-Zehnder interferometer, PBS: polarization beam splitter

Fs-laser inscribed (de)multiplexer

Various schemes for handling high-order fiber modes have been proposed previously. Compared with these traditional (de)multiplexers (e.g. phase plates, spatial light modulators), the photonic lantern shows distinct advantages of compact and cost effective for practical multi-mode fiber-optic communication applications. Here, we choose the three lowest-order modes (LP_{01}, LP_{11a} and LP_{11b}) as different orthogonal spatial modes to enable multi-mode-channel data transmission by photonic lantern. As shown in Fig. 2a, the photonic lantern is fabricated in a $20 \times 40 \times 1$ mm^3 glass-substrate chip by fs-laser direct writing technique. The high repetition rate Ytterbium-based laser provides a fs-laser beam (1030 nm wavelength, 200 kHz repetition rate, 234 fs pulse duration) for fabrication. A 300 nm linear slit and an objective are used to modify and focus the laser beam respectively. The fs-laser with a pulse energy of 900 nJ could change the refractive index of silica chip at a constant speed of 0.2 mm/s. The refractive index contrast ($\Delta n \approx 0.3\%$) in silica chip could confine the light within the waveguide for propagation. The waveguide is written twice to provide a smooth waveguide and higher refractive index contrast, which is conducive to reducing the waveguide propagation loss. As displayed in Fig. 2b, when the photonic lantern shows the function of mode multiplexing, it has three input ports and one output port. The cross-section diameter of the single-mode and multi-mode waveguides are 7 and 14 μm, respectively. The single-mode waveguide port spacing of 127 μm is set to match the interface of fiber array, allowing multiple mode channels to work simultaneously. The coupling method of silica chip adopts the edge coupling. The photo image of the fs-laser inscribed photonic lantern is shown in Fig. 3a, occupying an area of about 20×0.4 mm^2. Figure 3c illustrates the enlarged views of the multimode port (I) and three single-mode ports (II).

The photonic lantern could be regarded as two parts. First, the linearly aligned array of three single-mode ports is gradually remapped into a triangle array. The side length of the triangle is 40 μm, which is long-enough waveguide spacing to avoid waveguide coupling in this part. Then, they approach each other by different 3D trajectories and merge to form a triangle multi-mode output waveguide. In the process of waveguide approaching, the light of three waveguides could be converted and redistributed through evanescent wave coupling to form different super-modes at the multimode port. Based on the super-mode theory, the formed mode field of multimode port could be modulated
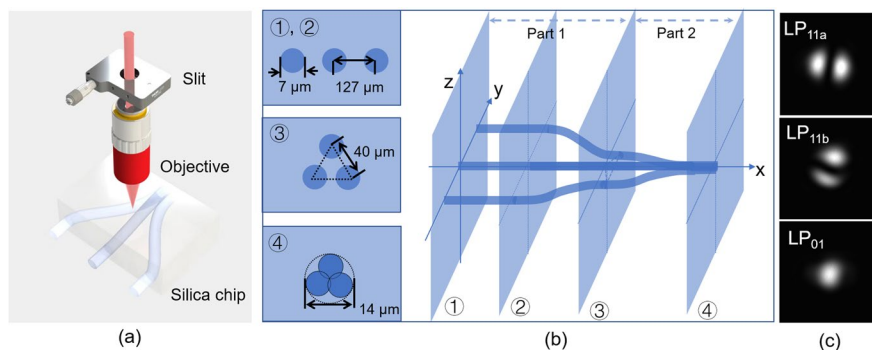

Fig. 2 Fs-laser inscribed (de)multiplexer. **a** Fs-laser direct writing structure of the 3D mode (de)multiplexer. **b** The schematic diagram and different cross sections of the photonic lantern. **c** The measured intensity profiles of LP_{11a}, LP_{11b} and LP_{01} modes
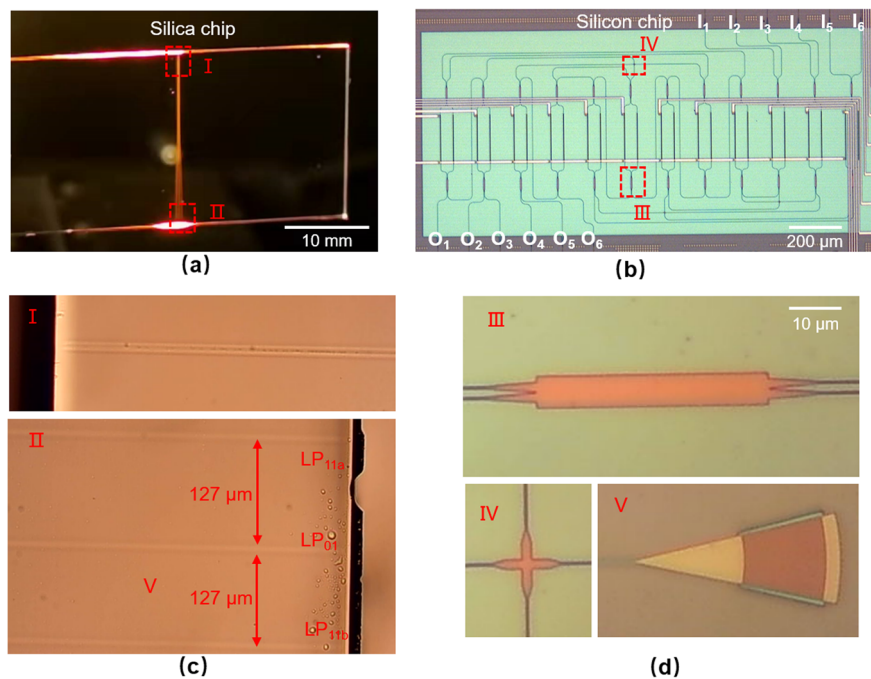
Fig. 3 Fabricated fs-laser inscribed (de)multiplexer silica chip and silicon switch array chip. **a** Measured photo image of the fabricated (de)multiplexing 3D silica chip by fs-laser direct writing technique. **b** Measured optical microscope of the fabricated 2D silicon switch array chip by the standard CMOS-compatible fabrication process. **c** The enlarged views of the multimode port (I) and three single mode ports (II) in the silica chip. **d** The enlarged views of the MMI (III), crossing (IV) and grating coupler(V) in the silicon chip

by changing the coupling strength of each waveguide. When the appropriate coupling parameters (waveguide spacing and coupling length) are selected, the super-mode field could be matched with the LP mode fields in the FMF. Therefore, the photonic lantern achieves a significant peculiarity of mode selectivity. As shown in Fig. 2c, the measured intensity profiles of three LP modes all have high purity. Furthermore, benefiting from the peculiarity of polarization independence, the photonic lantern could be simply formed as a 6-channel hybrid mode/polarization (de)multiplexer by introducing three fiber polarization beam splitters (PBSs), as displayed in Fig. 1a and c.

Silicon switch array

The flexible optical switching for mode/polarization channels in FMF is of great interest in grooming multi-mode fiber-optic communication networks. In the FMF-chip-FMF transmission and switching system, after mode/polarization multiplexing transmission through the first segment of FMF, the hybrid 6 mode/polarization channels are demultiplexed by the fs-laser inscribed demultiplexer silica chip together with fiber-based PBSs, the 6 outputs of which are coupled into the silicon switch array chip. After dynamic optical switching, the 6 channels are converted and multiplexed into 6 mode/polarization channels in the second segment of FMF for transmission by the fs-laser inscribed multiplexer silica chip. This indicates that the dynamic optical switching is equivalent to the hybrid mode/polarization switching. Here, the 6×6 non-blocking 2D silicon integrated

optical switch is utilized to accommodate 6 mode/polarization channels in the FMF, which implements the functions of 6-channel routing and 6×6 switching.

The non-blocking topology optical switch obeys the following rules: (1) the light injected into the input of any port can be destined to the output of any other port; (2) the light injected into the input of any one port is not allowed to guide to the output of the same port (output port contention); (3) the light should not be ingress and egress from the same port ("U" turn); (4) any internal links between an input and an output would never block the possible links between the remaining inputs and outputs [9]. It is worth mentioning that the used topology-optimized 6×6 non-blocking switch (depicted in Fig. 1c) possesses the advantages of fewer units, simpler topology and lower loss, compared with the traditional 6×6 Benes and Spanke-Benes optical switching topology [39, 40]. The topology-optimized 6×6 non-blocking switch contains only 12 2×2 switch units and 3 crossings. The loss of five switches and one crossing is the maximal insertion loss of the optimized 6×6 switch. The key 2×2 switch unit is an MZI that is composed of two 2×2 multimode interferometers (MMIs) and a phase shifter. Based on the thermo-optical effect, the MZI states of "Bar" and "Cross" could be switched arbitrarily by thermal tuning. The shallow-etched grating couplers are adopted in silicon chip. As shown in Fig. 3b, the measured optical microscope of the 6×6 non-blocking silicon switch array chip with a footprint of 1.8×0.8 mm^2 is fabricated by the standard CMOS-compatible fabrication process. Figure 3c illustrates the enlarged views of the MMI (III), crossing (IV) and grating coupler (V) in the silicon chip.

Device characterization

To characterize the performance, the mode/polarization multiplexer and demultiplexer are connected with a 150-m FMF by the edge coupling, which has 6 input ports and 6 output ports (corresponding to LP_{01x}, LP_{01y}, LP^a_{11x}, LP^a_{11y}, LP^b_{11x} and LP^b_{11y} mode/polarization channels, respectively). When light is launched into input ports one by one, lights from 6 output ports are all monitored simultaneously. Figure 4i and j show the normalized crosstalk matrixes of two sets of mode-division multiplexing and demultiplexing system with 150-m-long FMF before and after the silicon switch chip, respectively. Note that here the insertion loss refers to the total loss including the edge coupling of two input and output ports. It is shown that the two mode (de)multiplexing systems both have an approximate insertion loss of < 10 dB and crosstalk of < -15 dB, indicating that the performance of different (de) multiplexing chips are almost uniform. The device performance can be further improved by optimizing the fabrication technology.

The performance of the silicon-based integrated optical switch can be characterized by the transmission spectra. A broadband source is employed in the experiment. Figure 4a-f show the normalized transmission spectra for the 6×6 optical switch with a representative switching status (1−2, 2−4, 3−1, 4−3, 5−6, 6−5), with the light injected into different input port I_1, I_2, I_3, I_4, I_5, I_6, respectively. The measured average crosstalk among different switching ports is less than -20 dB, and the average insertion loss is less than 5 dB. Except for the insertion loss and crosstalk, the power consumption and switching speed are also important performance metrics in a switch system. Figure 4g shows the normalized transmission of the MZI cross port as a function of different heating powers. When the heating power is $P_1 = 12.61$ mW, the MZI exhibits the state of "Bar". Due
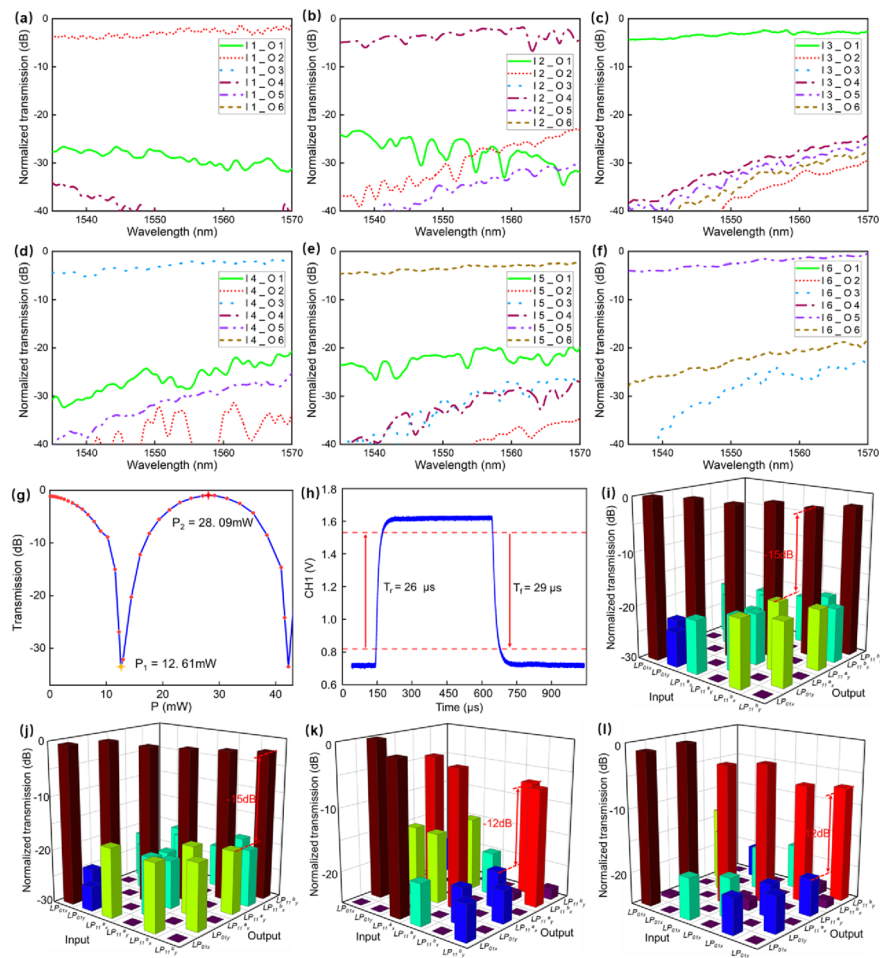
Fig. 4 Measured results of devices and FMF-chip-FMF system. **a**-**f** Measured transmission spectra for the 6 × 6 optical switch with a representative switching status (1−2, 2−4, 3−1, 4−3, 5−6, 6−5), with the light injected into different input port (**a**) I₁, (**b**) I₂, (**c**) I₃, (**d**) I₄, (**e**) I₅, (**f**) I₆, respectively. **g** Normalized transmission of the MZI cross port as a function of different heating powers. **h** Measured switching response of the MZI switch operating with different heating voltages. **i**, **j** Normalized crosstalk matrixes of two sets of mode-division multiplexing and demultiplexing system with 150-m-long FMF before and after the silicon switch chip. **k**, **l** Measured crosstalk matrixes for different mode/polarization channels of the whole FMF-chip-FMF mode/polarization transmission and switching system for the functions of switching and routing. **k** Switching function (1−2, 2−4, 3−1, 4−3, 5−6, 6−5). **l** Routing function (1−1, 1−2, 1−3, 1−4, 1−5, 1−6)

to the phase error introduced by the fabrication error, the MZI without heating may not be suitable to represent the "Cross" state. Therefore, the heating powers of $P_2 = 28.09$ mW is chosen to realize the function of optical switching. Figure 4h shows the measured switching response of the MZI switch operating with different heating voltages, which has a switching rise-time of 26 µs and a switching drop-time of 29 µs. Hence, a time of <30 µs could enable the system to switch from one switching status to another.

Experimental results

Based on the FMF-chip-FMF mode/polarization switching system constructed above, we further measure the system performance when passing through FMF transmission links, hybrid mode/polarization (de)multiplexers and silicon switch array chip with high-speed signals. In particular, in order to demonstrate the compatibility of the switching system with WDM signals, 16 wavelengths are used and fed into the system simultaneously. Shown in Fig. 5 is the experimental setup of the FMF-chip-FMF mode/polarization transmission and switching system, including the transmitter, the FMF-chip-FMF transmission and switching system, and the receiver.

As shown in Fig. 5b, at the transmitter, 16 wavelength channels with an approximately 0.8-nm channel spacing (from 1547.3 nm to 1558.9 nm) are combined by the WDM device. An arbitrary waveform generator (AWG) drives an optical I/Q modulator to modulate the light into a 30-Gbaud QPSK signal. The signal is divided into odd and even channels by a waveshaper, with one delayed by 100-m single-mode fiber (SMF) for data pattern decorrelation. The odd and even channels are then combined by a 50:50 optical coupler (OC). Two EDFAs are used to pre-amplify signals. The amplified signals are divided into 6 copies with different relative delays. Then the 6 signals are excited and multiplexed respectively into 6 different LP modes of FMF by using a fs-laser inscribed silica chip multiplexer. At the end of 150-m FMF, an inline PC is used to compensate for the crosstalk from moderate disturbance and FMF. With future improvement, the automatic polarization controller could replace the inline PC in the system to adapt to practical applications with disturbance [41–46]. The 6 LP modes transmitted over a short distance in the FMF are demultiplexed to 6 fundamental modes by another fs-laser inscribed silica chip demultiplexer, which are all injected into a silicon switch array chip by vertical grating coupling. After on-chip 6 × 6 optical switching, in the same way, the switched mode/polarization signals are multiplexed, coupled for MDM transmission,
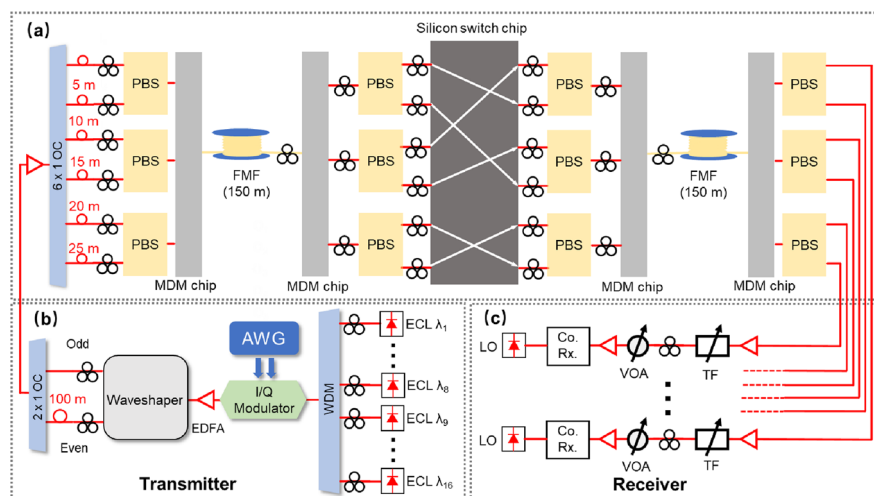

Fig. 5 Experimental setup for the FMF-chip-FMF mode/polarization switching system. **a** FMF-chip-FMF system. **b** Transmitter. **c** Receiver. ECL: external cavity laser; WDM: wavelength-division multiplexing; AWG: arbitrary waveform generator; EDFA: erbium-doped fiber amplifier; VOA: variable optical attenuator; Co. Rx.: coherent receiver

and then demultiplexed by another set of fs-laser inscribed silica chip multiplexer, 150-m FMF, and fs-laser inscribed silica chip demultiplexer. Finally, the multi-channel signals are sent to the receiver for coherent detection, as shown in Fig. 5c. The intradyne coherent detection is implemented by the integrated coherent receiver and local oscillator (LO) [47]. A real-time oscilloscope is used to detect electrical signals for offline processing. In the receiver digital signal processing (DSP), the received signals of each channel are resampled and any IQ non-orthogonality is compensated with Gram-Schmidt orthogonalization procedure (GSOP), then followed by a liner equalization and the carrier recovery algorithm to recover the signals.

Figure 4k and l show the measured crosstalk matrixes of the whole FMF-chip-FMF mode/polarization transmission and switching system for the functions of switching (1−2, 2−4, 3−1, 4−3, 5−6, 6−5) and routing (1–1, 1–2, 1–3, 1–4, 1–5, 1–6), respectively. It can be seen that the measured worst crosstalk of -12 dB corresponds to the high-order mode channel. The total loss of the system is approximately 34 dB, consisting of four 6×6 mode/polarization (de)multiplexers, a 6×6 silicon switch and two grating couplers. Furthermore, if different modes and polarizations of FMF could be (de) multiplexed by a silicon-based multimode coupler with low loss and low crosstalk, the entire system has great potential to be integrated on a silicon chip. Such an integrated system will obtain superior performance in terms of integration density, insertion loss and crosstalk.

Furthermore, we characterize the BER performance of the 6×6 non-blocking optical switch. Here the BER performance is evaluated by selecting a typical wavelength channel (1550.30 nm) in the switching experiment. The $I(O)_1$, $I(O)_2$, $I(O)_3$, $I(O)_4$, $I(O)_5$, $I(O)_6$ input (output) ports of the 6×6 silicon switch are connected to the LP^b_{11x}, LP^b_{11y}, LP^a_{11x}, LP^a_{11y}, LP_{01x} and LP_{01y} mode output (input) of the demultiplexer (multiplexer), respectively. The measured BERs as a function of the received OSNR for the switching status (1−2, 2−4, 3−1, 4−3, 5−6, 6−5, as illustrated in Fig. 1c) are shown in Fig. 6. The observed OSNR penalties of each mode/polarization switching channel at a BER of 3.8×10^{-3}
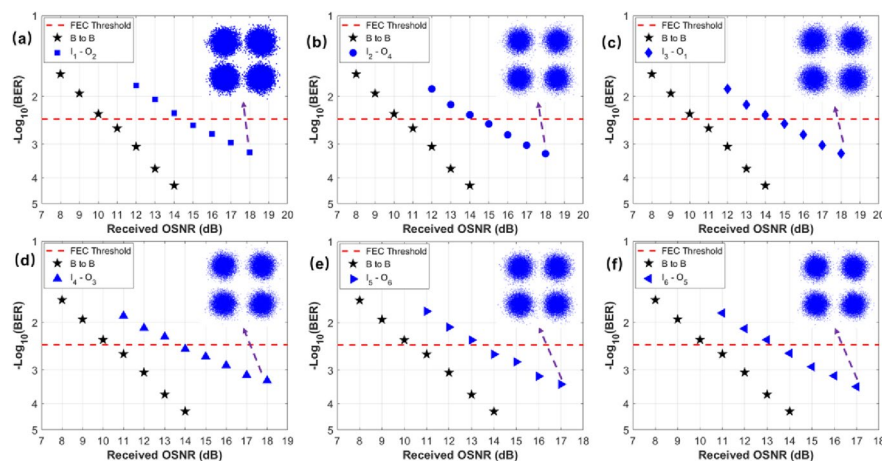

Fig. 6 Measured BER performance for the 6×6 optical switch. The switching status is **a** 1−2, **b** 2−4, **c** 3−1, **d** 4−3, **e** 5−6, **f** 6−5. The $I(O)_1$, $I(O)_2$, $I(O)_3$, $I(O)_4$, $I(O)_5$, $I(O)_6$ input (output) ports of the 6×6 silicon switch are connected to the LP^b_{11x}, LP^b_{11y}, LP^a_{11x}, LP^a_{11y}, LP_{01x} and LP_{01y} mode output (input) of the demultiplexer (multiplexer), respectively. The insets show the typical constellations of QPSK signals

(7% hard-decision forward-error correction (HD-FEC) threshold) are about 2.8 ~ 3.8 dB compared to the back-to-back (B-B) case. The insets in Fig. 6 are the constellation diagrams of the recovered QPSK signals. The observed OSNR penalties differ from each other for different channels, which might be ascribed to different crosstalk and link loss of mode/polarization channels from the mode (de)multiplexer. As shown in Fig. 6, the relatively larger OSNR penalties of > 3 dB are measured for high-order mode (LP^a_{11} and LP^b_{11}) channels, which are consistent with the measured crosstalk of mode (de)multiplexer and FMF-chip-FMF system mentioned above.

We also characterize the BER performance of the multi-port router. Different wavelengths are selected in the BER measurement of each channel to better exhibit the WDM compatibility of the system. The measured BER performance as a function of the received OSNR for 6 representative multi-port routing status (1−1 @ 1548.2 nm, 1−2 @ 1550.3 nm, 1−3 @ 1552.65 nm, 1−4 @ 1553.55 nm, 1−5 @ 1555.8 nm, 1−6 @ 1558.1 nm) are shown in Fig. 7. The observed OSNR penalties for multi-port routing status at a BER of 3.8×10^{-3} (7% HD-FEC threshold) are about 3 ~ 4.5 dB compared to the B-B case. Similarly, the relatively low OSNR penalties are measured for low-order mode (LP_{01}) channels due to their low crosstalk and loss. Besides, one can clearly see that different wavelength channels achieve BER less than 3.8×10^{-3}, showing the favorable WDM compatibility. The obtained results shown in Figs. 6 and 7 with impressive performance indicate the successful implementation of the WDM-compatible hybrid mode/polarization transmission, switching and routing system with FMFs, fs-laser inscribed silica (de) multiplexing chip and silicon switch array chip.
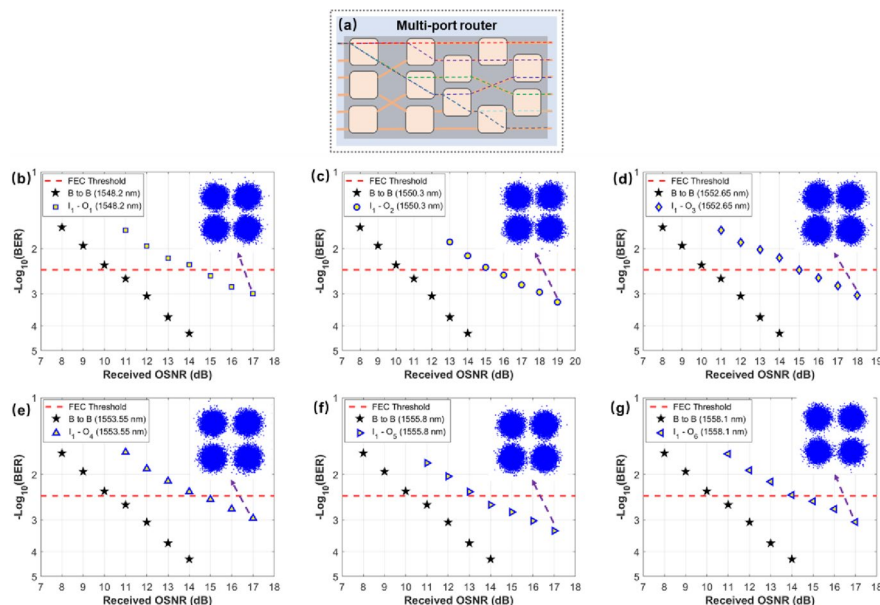

Fig. 7 Measured BER performance for the optical router. **a** Schematic illustration of the multi-port router. The router paths are **b** 1−1 @ 1548.2 nm, **c** 1−2 @ 1550.3 nm, **d** 1−3 @ 1552.65 nm, **e** 1−4 @ 1553.55 nm, **f** 1−5 @ 1555.8 nm, **g** 1−6 @ 1558.1 nm. The insets show the typical constellations of QPSK signals

Conclusion

In summary, a WDM-compatible FMF-chip-FMF mode/polarization transmission and switching system is built and demonstrated in this work. This transmission and switching system, consisting of two segments of 150-m FMF links for short-reach MDM data transmission, a 6×6 non-blocking silicon switch array chip, and several fs-laser inscribed mode/polarization (de)multiplexer silica chips for coupling between FMFs and silicon chip, implements various functions of transmission, (de)multiplexing, switching and routing for hybrid mode/polarization multiplexing signals. After topology optimization, the 6×6 non-blocking silicon switch with fewer units has a simplified structure and lower loss. By combining the 6-channel mode/polarization (de)multiplexer, the 6×6 silicon switch shows a crosstalk of < -12 dB for both switching and routing functions. By using 30-Gbaud QPSK signals over 16 WDM channels, the WDM-compatible FMF-chip-FMF mode/polarization transmission and switching system is demonstrated in the experiment with impressive performance. It is believed that the demonstrated WDM-compatible FMF-chip-FMF mode/polarization transmission and switching system may pave the way for future grooming optical switching networks.

Abbreviations

FMFs	Few-mode fibers
3D	3-Dimensional
2D	2-Dimensional
WDM	Wavelength-division multiplexing
SOI	Silicon-on-insulator
CMOS	Complementary metal-oxide semiconductor
PDM	Polarization-division multiplexing
EDFA	Erbium-doped fiber amplifier
SMF	Single-mode fiber
SDM	Space-division multiplexing
MCF	Multi-core fiber
MDM	Mode-division multiplexing
QPSK	Quadrature phase-shift keying
OSNR	Optical signal-to-noise ratio
BER	Bit-error rate
LP	Linear polarization
PC	Polarization controller
MZI	Mach-Zehnder interferometer
PBS	Polarization beam splitter
AWG	Arbitrary waveform generator
OC	Optical coupler
LO	Local oscillator
DSP	Digital signal processing
GSOP	Gram-Schmidt orthogonalization procedure
HD-FEC	Hard-decision forward-error correction
B-B	Back-to-back

Availability of data and materials
The datasets used and analysed during the current study are available from the corresponding author on reasonable request.

Declarations

Ethics approval and consent to participate
There is no ethics issue for this paper.

Consent for publication
All authors agreed to publish this paper.

Competing interests
The authors declare that they have no competing interests.

References
1. Namiki S, Hasama T, Ishikawa H. Optical signal processing for energy-efficient dynamic optical path networks. In: 36th European Conference and Exhibition on Optical Communication (ECOC). 2010. p. 1–6.
2. Willner A, Khaleghi S, Chitgarha M, Yilmaz O. All-optical signal processing. J Lightwave Technol. 2014;32:660–80.
3. Shacham A, Bergman K, Carloni L. Photonic networks-on-chip for future generations of chip multiprocessors. IEEE Trans Comput. 2008;57:1246–60.
4. Yoo S. Optical packet and burst switching technologies for the future photonic internet. J Lightwave Technol. 2006;24:4468–92.
5. Zheng S, Long Y, Gao D, Luo Y, Wang J. Chip-scale reconfigurable optical full-field manipulation: enabling a compact grooming photonic signal processor. ACS Photonics. 2020;7:1235–45.
6. Cao X, Zheng S, Long Y, Ruan Z, Luo Y, Wang J. Mesh-structure-enabled programmable multitask photonic signal processor on a silicon chip. ACS Photonics. 2020;7:2658–75.
7. Wonfor A, Wang H, Penty R, White I. Large port count high-speed optical switch fabric for use within datacenters. J Opt Commun Netw. 2011;3:A32–9.
8. Cheng Q, Rumley S, Bahadori M, Bergman K. Photonic switching in high performance datacenters. Opt Express. 2018;26:16022–43.
9. Chen Q, Zhang F, Ji R, Zhang L, Yang L. Universal method for constructing N-port non-blocking optical router based on 2 × 2 optical switch for photonic networks-on-chip. Opt Express. 2014;22:12614–27.
10. Chen L, Chen Y. Compact, low-loss and low-power 8×8 broadband silicon optical switch. Opt Express. 2012;20:18977–85.
11. Dong P, Zhang L, Dai D, Shi Y. All-optical switching of silicon nanobeam cavities with an ultra-compact heater utilizing the photothermal effect. ACS Photonics. 2021;9:197–202.
12. Suzuki K, Tanizawa K, Matsukawa T, Cong G, Kim S, Suda S, Ohno M, Chiba T, Tadokoro H, Yanagihara M, Igarashi Y, Masahara M, Namiki S, Kawashima H. Ultra-compact 8 × 8 strictly-non-blocking Si-wire PILOSS switch. Opt Express. 2014;22:3887–94.
13. Kwack M, Tanemura T, Higo A, Nakano Y. Monolithic InP strictly non-blocking 8×8 switch for high-speed WDM optical interconnection. Opt Express. 2012;20:28734–41.
14. Takiguchi M, Takemura N, Tateno K, Nozaki K, Sasaki S, Sergent S, Kuramochi E, Wasawo T, Yokoo A, Shinya A, Notomi M. All-optical InAsP/InP nanowire switches integrated in a Si photonic crystal. ACS Photonics. 2020;7:1016–21.
15. Seok T, Quack N, Han S, Wu M. 50×50 Digital silicon photonic switches with MEMS-actuated adiabatic couplers. In: Optical Fiber Communication Conference (OFC). 2015. p. M2B.4.
16. Shi Y, Zhang Y, Wan Y, Yu Y, Zhang Y, Hu X, Xiao X, Xu H, Zhang L, Pan B. Silicon photonics for high-capacity data communications. Photonics Res. 2022;10:A106–34.
17. Shi W, Tian Y, Gervais A. Scaling capacity of fiber-optic transmission systems via silicon photonics. Nanophotonics. 2020;9:4629–63.
18. Winzer P, Neilson D, Chraplyvy A. Fiber-optic transmission and networking: the previous 20 and the next 20 years. Opt Express. 2018;26:24190–239.
19. Li X, Yu J, Zhang J, Li F, Xu Y, Zhang Z, Xiao J. Fiber-wireless-fiber link for 100-Gb/s PDM-QPSK signal transmission at W-Band. IEEE Photon Technol Lett. 2014;26:1825–8.
20. Richardson D, Fini J, Nelson L. Space-division multiplexing in optical fibres. Nat Photonics. 2013;7:354–62.
21. Mitra P, Stark J. Nonlinear limits to the information capacity of optical fibre communications. Nature. 2001;411:1027–30.
22. Wang J, Yang J, Fazal I, Ahmed N, Yan Y, Huang H, Ren Y, Yue Y, Dolinar S, Tur M, Willner A. Terabit free-space data transmission employing orbital angular momentum multiplexing. Nat Photonics. 2012;6:488–96.
23. van Uden R, Correa R, Lopez E, Huijskens F, Xia C, Li G, Schülzgen A, Waardt H, Koonen A, Okonkwo C. Ultra-high-density spatial division multiplexing with a few-mode multicore fibre. Nat Photonics. 2014;8:865–70.
24. Stuart H. Dispersive multiplexing in multimode optical fiber. Science. 2000;289:281–3.
25. Rademacher G, Puttnam B, Luís R, Eriksson T, Fontaine N, Mazur M, Chen H, Ryf R, Neilson D, Sillard P, Achten F, Awaji Y, Furukawa H. Peta-bit-per-second optical communications system using a standard cladding diameter 15-mode fiber. Nat Commun. 2021;12:4238.

26. Winzer P. Making spatial multiplexing a reality. Nat Photonics. 2014;8:345–8.
27. Kawaguchi Y, Tsutsumi K. Mode multiplexing and demultiplexing devices using multimode interference couplers. Electron Lett. 2002;38:1.
28. Zhang L, Lu D, Li Z, Pan B, Zhao L. C-band fundamental/first-order mode converter based on multimode interference coupler on InP substrate. J Semicond. 2016;37:124005.
29. Uematsu T, Ishizaka Y, Kawaguchi Y, Saitoh K, Koshiba M. Design of a compact two-mode multi/demultiplexer consisting of multimode interference waveguides and a wavelength-insensitive phase shifter for mode-division multiplexing transmission. J Lightwave Technol. 2012;30:2421.
30. Riesen N, Love J. Design of mode-sorting asymmetric Y-junctions. Appl Opt. 2012;51:2778.
31. Chen W, Wang P, Yang J. Mode multi/demultiplexer based on cascaded asymmetric Y-junctions. Opt Express. 2013;21:25113.
32. Xing J, Li Z, Xiao X, Yu J, Yu Y. Two-mode multiplexer and demultiplexer based on adiabatic couplers. Opt Lett. 2013;38:3468.
33. Wang J, He S, Dai D. On-chip silicon 8-channel hybrid (de) multiplexer enabling simultaneous mode-and polarization-division-multiplexing. Laser Photon Rev. 2014;8:L18.
34. Li K, Cao X, Wan Y, Wu G, Wang J. Fundamental analyses of fabrication-tolerant high-performance silicon mode (de) multiplexer. Opt Express. 2022;30:22649–60.
35. Ren F, Li J, Hu T, Tang R, Yu J, Mo Q, He Y, Chen Z, Li Z. Cascaded mode-division-multiplexing and time-division-multiplexing passive optical network based on low mode-crosstalk FMF and mode MUX/DEMUX. IEEE Photonics J. 2015;7:1.
36. Leon-Saval S, Argyros A, Bland-Hawthorn J. Photonic lanterns: a study of light propagation in multimode to single-mode converters. Opt Express. 2010;18:8430.
37. Tong Y, Zhou W, Wu X, Tsang H. Efficient mode multiplexer for few-mode fibers using integrated silicon-on-insulator waveguide grating coupler. IEEE J Quantum Electron. 2019;56:1.
38. Zhang Z, Tong Y, Wang Y, Tsang H. Nonparaxial mode-size converter using an ultracompact metamaterial Mikaelian lens. J Lightwave Technol. 2020;39:2077.
39. Zheng D, Doménech J, Pan W, Zou X, Yan L, Pérez D. Low-loss broadband 5×5 non-blocking Si3N4 optical switch matrix. Opt Lett. 2019;44:2629–32.
40. Xing J, Li Z, Zhou P, Xiao X, Yu J, Yu Y. Nonblocking 4×4 silicon electro-optic switch matrix with push–pull drive. Opt Lett. 2013;38:3926–9.
41. Wang T, Wang T, Lan S, Jiang J, Liu T. A novel method of polarization state control for polarization division multiplexing system. Chin Opt Lett. 2008;6(6):812–4.
42. Yang Y, Geng C, Li F, Huang G, Li X. Coherent polarization beam combining approach based on polarization controlling in fiber devices. IEEE Photon Technol Lett. 2017;29:945–8.
43. Lin Z, Dadalyan T, Villers S, Galstian T, Shi W. Chip-scale full-stokes spectropolarimeter in silicon photonic circuits. Photon Res. 2020;8:864–74.
44. Zhou H, Zhao Y, Wei Y, Li F, Dong J, Zhang X. All-in-one silicon photonic polarization processor. Nanophotonics. 2019;8:2257–67.
45. Noe R, Koch B, Mirvoda V, Hidayat A, Sandel D. 38-krad/s 3.8-Grad broadband endless optical polarization tracking using LiNbO3 device. IEEE Photon Technol Lett. 2019;21:1220–2.
46. Koch B, Noé R, Sandel D, Mirvoda V. Versatile endless optical polarization controller/tracker/demultiplexer. Opt Express. 2014;22:8259–76.
47. Ezra I, Alan P, Daniel J, Joseph M. Coherent detection in optical fiber systems. Opt Express. 2008;16:753–91.

Publisher's Note

Springer Nature remains neutral with regard to jurisdictional claims in published maps and institutional affiliations.